Available online at www.sciencedirect.com
ScienceDirect
Trans. Nonferrous Met. Soc. China 30(2020) 1335−1346
Transactions of Nonferrous Metals Society of China
www.tnmsc.cn

Influence of Al addition on microstructures of Cu−B alloys and Cu−ZrB_2 composites

Hai-min DING[1], Wen-zhi MIAO[1], Xiao-wei HUANG[1], Qing LIU[1], Xiao-liang FAN[1], Hui-qiang WANG[2], Kai-yu CHU[1], Chun-yan LI[1]

1. School of Energy, Power and Mechanical Engineering, North China Electric Power University, Baoding 071003, China;
2. College of Mechanical and Electric Engineering, Hebei Agricultural University, Baoding 071001, China

Received 29 September 2019; accepted 20 March 2020

Abstract: The influence of Al addition on the microstructure of Cu−B alloys and Cu−ZrB_2 composites was investigated using scanning electron microscopy, X-ray diffraction and first-principles calculation. The results show that the eutectic B in Cu−B alloys can be modified by Al from coarse needles to fine fibrous structure and primary B will form in hypoeutectic Cu−B alloys. As for Cu−ZrB_2 composites, Al can significantly refine and modify the morphology of ZrB_2 as well as improve its distribution, which should be due to its selective adsorption on ZrB_2 surfaces. The first-principles calculation results indicate that Al is preferentially adsobed on ZrB_2 $(1\bar{2}10)$, then on ZrB_2 $(10\bar{1}0)$, and finally on ZrB_2 (0001). As a result, smaller sized ZrB_2 with a polyhedron-like, even nearly sphere-like morphology, can form. Due to Al addition, the hardness of Cu−ZrB_2 composites is greatly enhanced, but the electrical conductivity of the composites is seriously reduced.

Key words: Cu−B alloys; Cu matrix composites; modification effect; microstructures

1 Introduction

Cu and its alloys have been widely used in many fields due to their excellent mechanical properties, electrical and thermal conductivities [1−3]. Nowdays, the requirements for Cu alloys are getting higher with the continuous development of related industries. In order to meet the increasing requirements, one of the widely used methods is reinforcement of Cu alloys by hard secondary phases [4,5]. In this case, the property of the reinforcement phases is one of the key factors to develope high performance composites [6,7]. Oxides, carbides and borides are considered to be good candidates as reinforcements due to their high melting point, high hardness, and good corrosion resistance and so on [8−11]. Among them, it has been reported that transition metal borides possess much higher electrical conductivity, lower thermal expansion coefficient and better wettability with molten copper, which makes them more suitable for fabrication of high strength and conductivity Cu matrix composites [12−14]. As one kind of the transition metal borides, ZrB_2 has become an emerging candidate to develop Cu matrix composites [15−17]. It has been found that, compared with TiB_2 which has been widely used in Cu matrix composites, ZrB_2 possesses better wettability with molten Cu. Moreover, the solid solubility of Zr is very low in Cu matrix and there are few intermediate phases in Cu−Zr−B system,

Foundation item: Project (51774212) supported by the National Natural Science Foundation of China; Projects (E2019502060, E2019502057) supported by the Natural Science Foundation of Hebei Province, China
Corresponding author: Hai-min DING, Tel: +86-312-7525404, E-mail: haimin_ding@163.com;
Hui-qiang WANG, Tel: +86-312-7521580, E-mail: whq@hebau.edu.cn
DOI: 10.1016/S1003-6326(20)65300-6

which may offer a good interface bond in the ZrB_2/Cu composites [18−20]. For example, ZHANG et al [19] have prepared the Cu−ZrB_2 composites with hardness higher than HV 120 and electrical conductivity higher than 70% IACS using a liquid metallurgy route; recently, they further prepared the Cu−ZrB_2 composites with hardness higher than HV 100 and electrical conductivity higher than 85% IACS by hot-pressed sintering [20]. The Cu−ZrB_2 composites with hardness of HV 180 and the electrical conductivity of 42% IACS have also been prepared through green compact laser sintering by STASIC et al [21].

In our previous work, Cu−ZrB_2 composites with high strength and good conductivity were also successfully prepared by in-situ synthesizing ZrB_2 in Cu melts [22]. However, it is found that the microstructure uniformity of the prepared Cu−ZrB_2 composites was very poor. The synthesized ZrB_2 particles tend to be seriously aggregated. In addition, the particle size was uneven and ranged from less than 1 μm to more than 10 μm. The non-uniform microstructures of the Cu−ZrB_2 composite seriously deteriorated the performance.

Recently, it is found that the addition of Al can effectively improve the microstructures of Cu−ZrB_2 composites prepared by in-situ synthesizing ZrB_2 in Cu melts. The detailed results are present in this work and its mechanism is also investigated. The work provids a useful method for controlling the microstructures of in-situ synthsized ZrB_2 particles in Cu melts.

2 Experimental

Cu pieces(>99.9%), Zr pieces (>99.0%), Al pieces (>99.7%) and Cu−5B master alloy were used as starting materials. The main purpose of this work was to study the influnce of Al on the microstructures of Cu−ZrB_2 composites; however, because the ZrB_2 was in-situ synthsized by adding Zr into Cu−B or Cu−Al−B melts, Cu−0.75B, Cu−2Al−0.75B and Cu−6Al−0.75B master alloys were firstly prepared to examine the influence of Al addition on the microstructure of Cu−B master alloys.

Then Cu−B or Cu−Al−B master alloys were then used to prepare Cu−ZrB_2 composites. The Cu−3.15Zr−0.75B with Zr:B mole ratio of 1:2 was firstly prepared by adding Zr into Cu−B melts. Then, the other five kinds of composites with different Al contents which were Cu−1Al−3.15Zr−0.75B, Cu−2Al−3.15Zr−0.75B, Cu−3Al−3.15Zr−0.75B, Cu−4Al−3.15Zr−0.75B and Cu−6Al−3.15Zr−0.75B were prepared. During the prepartion, the related Cu−Al−B master alloys were firstly melt in quartz crucible by a SPG-20B high frequency induction heating furnace to 1200−1300 °C. Then, Zr was added into the Cu−Al−B melts and held for about 60 s. After that, the melt was poured into a steel die mould to obtain the composities.

Specimens were then cut from the as-cast composites to carry out grinding and polishing through standard routines. The microstructures of the samples were then investigated by a metallurgical microscope, an X-ray diffraction (XRD, Moldel D/Max 2500 PC, Rigaku,Japan) with Cu K_α radiation and a scanning electron microscope (SEM) attached with an energy dispersive X-ray spectroscopy (EDS). To further study the morphologies of the in-situ synthsized ZrB_2, the Cu−ZrB_2 composites were also deeply etched in 18 vol.% phosphoricacid solution for 30 s under the current of 5 A to etch off the surface Cu matrix and expose the ZrB_2 particles. Then the etched samples were analyzed by SEM.

3 Results and discussion

3.1 Influence of Al on microstructures of Cu−B master alloys

The influence of Al on the microstructures of Cu−B master alloys was firstly studied and the results are shown in Fig. 1. Figure 1(a) indicates that Cu−0.75B master alloy is composed of Cu matrix and euthectic B phase which distributes along Cu grains boundry. The euthectic B is needle-like as shown in Fig. 1(b). After addtion of 2 wt.% Al, B is still in the form of eutectic phase in Cu−2Al−0.75B and no Al-containing boron phase, such as AlB_2, is found. However, the morphology of eutectic B has been modified from coarse needle-like into fine fibrous structure, as shown in Figs. 1(c) and (d). Increasing the addtion amount of Al to 6 wt.%, the microstructure of Cu−0.75B is further modified. It is noticed from Figs. 1(e) and (f) that there is a new particle-like phase and the size of the particles ranges from 5 to 10 μm. The insert in Fig. 1(f) demostrates that the particle-like phase is actually polyhedral.

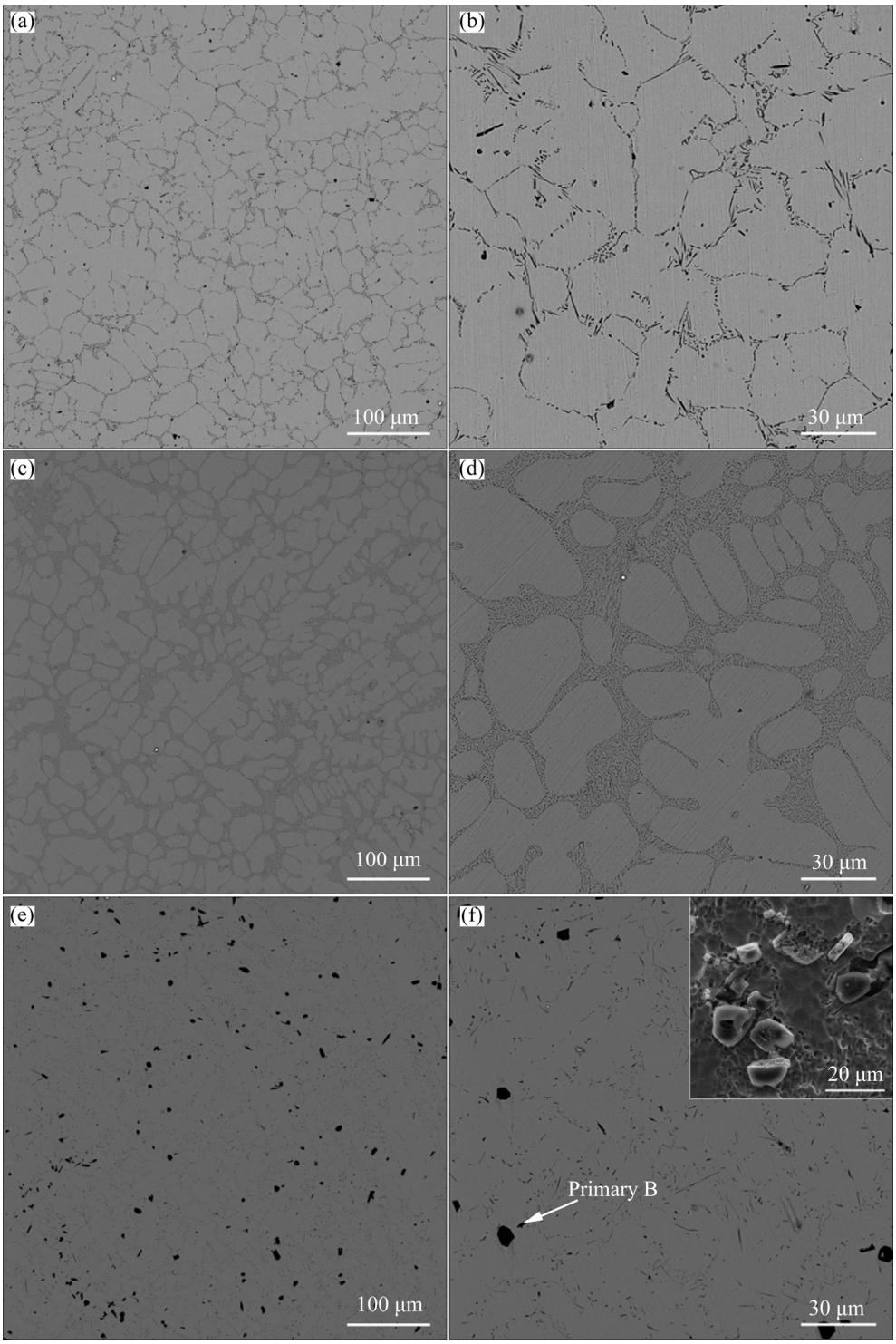

Fig. 1 Microstructures of Cu−B and Cu−Al−B master alloys: (a, b) Cu−0.75B; (c, d) Cu−2Al−0.75B; (e, f) Cu−6Al−0.75B (Insert figure in Fig. 6(f): exposed primary B after deeply etching)

EDS results given in Fig. 2 confirm that the particles mainly contain B as well as a slight amount of Al and Cu, which indicates that the particles should be the primary B [23]. According to the Cu−B phase diagram given in Fig. 3, the eutectic composition of Cu−B alloy is about 2.5 wt.% B. Therefore, the presence of primary B phase in Cu−6Al−0.75B proves that Al has a strong induction effect on the precipation of primary B. In addition, compared with Cu−2Al−0.75B, the eutectic B phase is much less in Cu−6Al−0.75B due to the formation of primary B phase and its size is

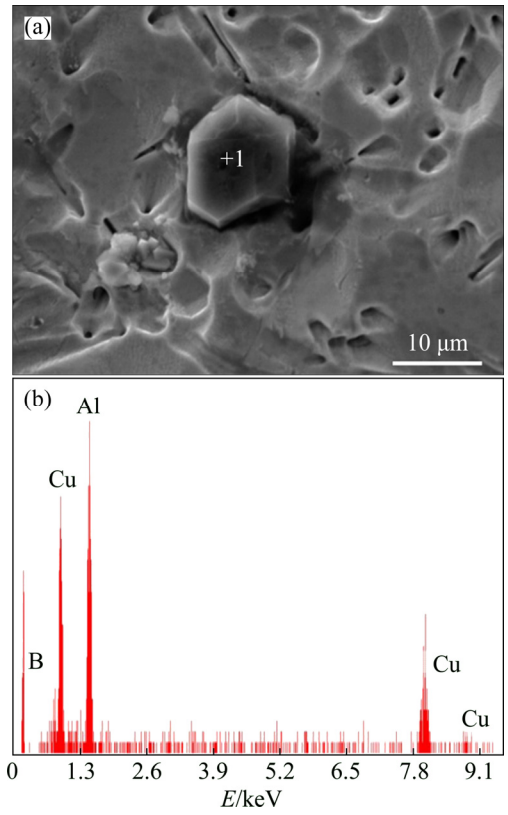

Fig. 2 EDS analysis results of primary B: (a) SEM image of deeply etching sample; (b) EDS analysis result of Point 1

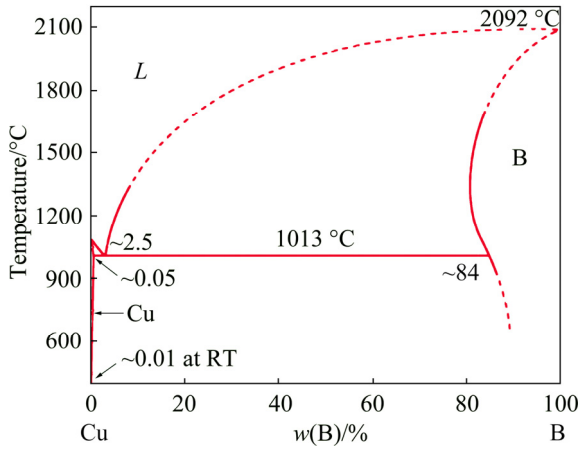

Fig. 3 Phase diagram of Cu−B alloy

much smaller than that in Cu−0.75B, which further confirms the modifcation effect of Al on eutectic B phase. Besides primary and eutectic B phase, other B-containing phases are hardly found in Cu−6Al−0.75B master alloy.

The above results demonstrate that Al has a significant modification effect on eutectic B phase in Cu−B master alloys and strong induction effect on the formation of primary B. It is interesting to notice that the modification effect of Al on euthectic and primary B of Cu−B alloys is very similar to that of Sr and P on eutectic and primary Si of Al−Si alloys. The modification effects of Sr and P on Al−Si alloys have been extensivly studied. As to the modification effect of Sr on eutectic Si, although there are still different suggested models, the commonly accepted one is that Sr tends to selectively adsorb on the growth surfaces of Si crystal and then retards the Si growth and changes the growth direction [24,25]. As to induction effect on the precipation of primary B by P, it has been confirmed that P will react with Al to form AlP particle which has a very simliar crsytal structure to primary Si and therefore can be an excellent heterogeneous nucleation site for primary Si, as a result, primary Si can be formed in hypoeutectic Al−Si alloys [26,27]. It is deduced that the modification mechanism of Al on B phase of Cu−B master alloys is same to that of Sr and P on Si. Based on the above results, it is considered that, Al tends to adsorb on the growth surfaces of eutectic B and retards its growth. As a result, the coarse eutectic B will be modified into fine fibrous structure. When there is sufficient Al in Cu−B melts, some small Al-containing particles that are most likely to the Al−B phase are formed in the melts or during the solidificaiton. These particles can act as nucleation sites for B phase, which is the reason for the formation of primary B in hypoeutectic Cu−6Al−0.75B master alloy. Unlike Sr and P which will interfere each other, the formation of Al-containing particles will not interfere the modification effect of Al on eutectic B, as a result, the united modification on both eutectic and primary B can be realized, like that in Cu−6Al−0.75B master alloy.

3.2 Influence of Al on microstructures of Cu−ZrB_2 composites

Then Cu−ZrB_2 composites were prepared by adding Zr into Cu−B or Cu−Al−B melts to study the influence of Al addition on the microstructures of Cu−ZrB_2 composites. Figure 4 shows the XRD patterns of the prepared Cu−3.15Zr−0.75B, Cu−1Al−3.15Zr−0.75B, Cu−2Al−3.15Zr−0.75B, Cu−3Al−3.15Zr−0.75B, Cu−4Al−3.15Zr−0.75B and Cu−6Al−3.15Zr−0.75B composites, respectively. It can be seen that the composites mainly consist of Cu phase (α-Cu phase in Al-containing samples)

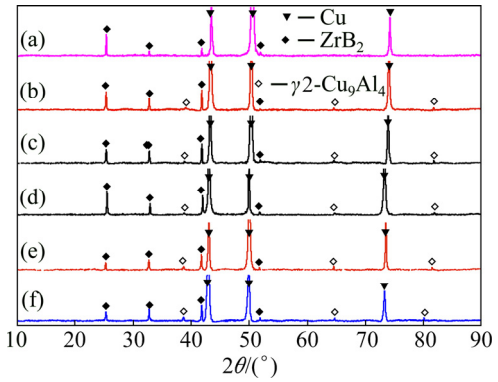

Fig. 4 XRD patterns of as−cast composites: (a) Cu−3.15Zr−0.75B; (b) Cu−1Al−3.15Zr−0.75B; (c) Cu−2Al−3.15Zr−0.75B; (d) Cu−3Al−3.15Zr−0.75B; (e) Cu−4Al−3.15Zr−0.75B; (f) Cu−6Al−3.15Zr−0.75B

and ZrB_2 phases, as well as some $\gamma 2$ phase (Cu_9Al_4) in Al-containing samples. No other B-containing phase has been detected. The results indicate that ZrB_2 has been successfully synthesized in all the composites.

Figure 5 shows the metallurgical micrographs of the composites. It can be seen that there are amounts of particles in Cu matirx in all the samples. Based on the XRD results, these particles should be in-situ synthesized ZrB_2. It is found from Fig. 5(a) that the distribution of ZrB_2 in Cu−3.15Zr−0.75B is not uniform and most of the ZrB_2 particles have been aggregated into agglomerations. After addition of Al, it is noticed that the distribution of ZrB_2 is signifcantly improved. According to Fig. 5(b),

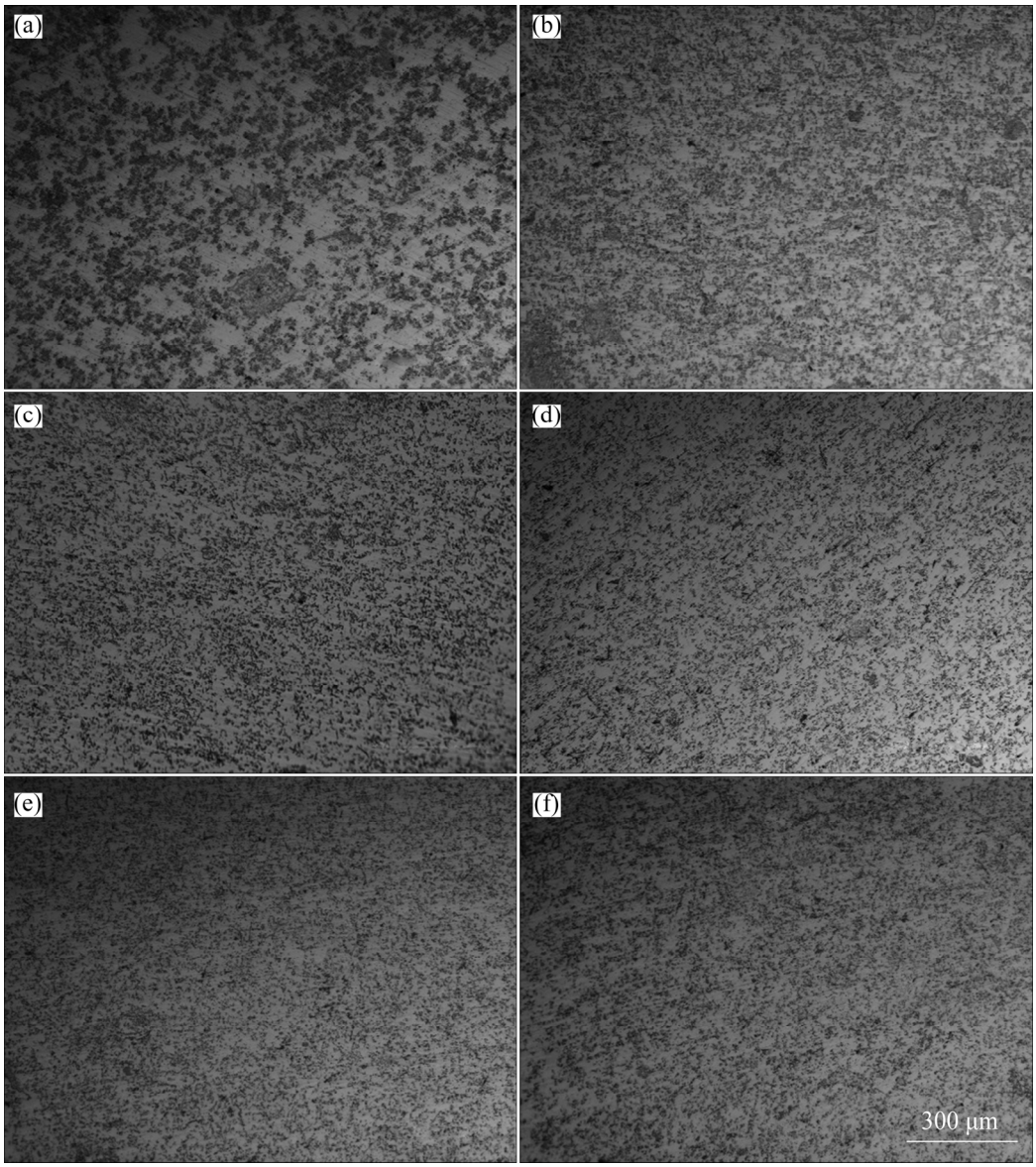

Fig. 5 Microstructures of as−cast composites: (a) Cu−3.15Zr−0.75B; (b) Cu−1Al−3.15Zr−0.75B; (c) Cu−2Al−3.15Zr−0.75B; (d) Cu−3Al−3.15Zr−0.75B; (e) Cu−4Al−3.15Zr−0.75B; (f) Cu−6Al−3.15Zr−0.75B

the ZrB_2 distribution is more uniform in Cu−1Al−3.15Zr−0.75B than that in Cu−3.15Zr−0.75B. The effect of Al on the ZrB_2 distribution is more obvious with Al content increasing. It is found from Figs. 5(c−f) that ZrB_2 is much more uniformly distributed in Cu−2Al−3.15Zr−0.75B, Cu−3Al−3.15Zr−0.75B, Cu−4Al−3.15Zr−0.75B and Cu−6Al−3.15Zr−0.75B compoistes and the large agglomerations can be hardly found, especially for the composites of Cu−4Al−3.15Zr−0.75B and Cu−6Al−3.15Zr−0.75B. Furthermore, the size of in-situ synthszied ZrB_2 is also decreased after Al addition.

In order to further examine the distribution and size as well as morphologies of ZrB_2, the prepared composites were deeply etched to remove the Cu matrix and expose ZrB_2. The microstructures of the etched samples are shown in Fig. 6. It is more obviously observed from Fig. 6(a) that the ZrB_2 particles are seriously aggregated in Cu−3.15Zr−0.75B composite to form agglomerations with different sizes and some are even larger than 100 μm. After addtion of 1 wt.% Al, as given in Fig. 6(b), although there are still some ZrB_2 agglomerations, both the quantity and size of ZrB_2 agglomerations are remarkably decreased , further confirming that Al addition can imporve the ZrB_2 distribution. By increasing Al amount, the modification effect becomes more significant. Like the results shown in Fig. 5, it can be seen from Figs. 6(c−f) that the large agglomerations almost disappeare and ZrB_2 is uniformly distributed in the Cu matrix after the addition of more than 2 wt.% Al.

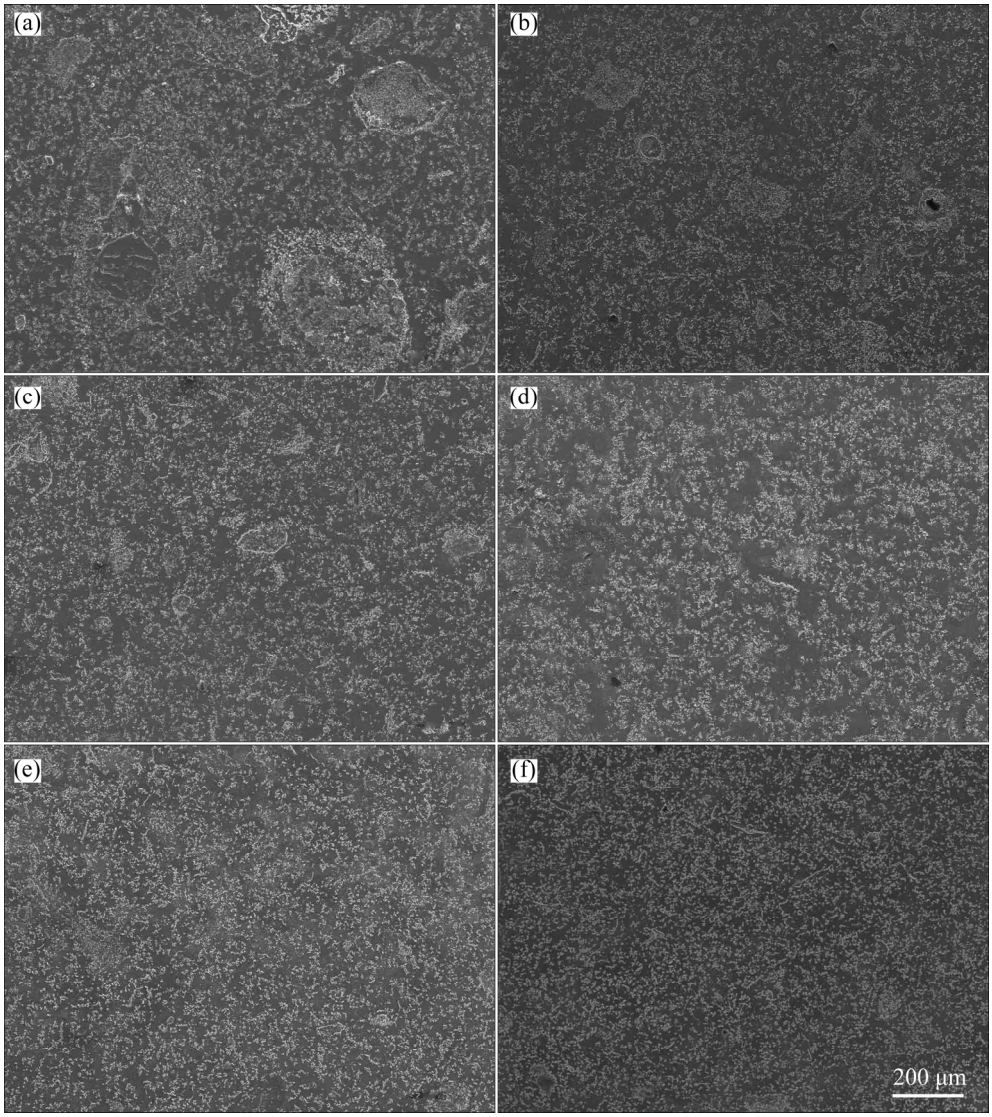

Fig. 6 Microstructures of deeply etched composites: (a) Cu−3.15Zr−0.75B; (b) Cu−1Al−3.15Zr−0.75B; (c) Cu−2Al−3.15Zr−0.75B; (d) Cu−3Al−3.15Zr−0.75B; (e) Cu−4Al−3.15Zr−0.75B; (f) Cu−6Al−3.15Zr−0.75B

In addition, it is also confirmed from Fig. 6 that, besides the distribution improvement, the addtion of Al has also decreased the size of ZrB_2 and changed the ZrB_2 morphologies, which can be more obviously observed from the microstructures of the ZrB_2 shown in Fig. 7. Figure 7(a) demonstrates that the size of ZrB_2 in Cu−3.15Zr−0.75B composite ranges from less than 1μm to larger than 10 μm. The size distribution was statistically measured and the result is shown in Fig. 8(a). It can be seen that about 45.72% ZrB_2 particles are larger than 2 μm and the mean size is about 2.34 μm. Moreover, most of ZrB_2 in Cu−3.15Zr−0.75B composite is plates with small height-to-diameter ratio and most of them, especailly the smaller one, are regular hexagonal plates. It is known that ZrB_2 has a hexagonal AlB_2-type structure with *P6*/*mmm* space group. For the crystal with AlB_2-type structure, the growth rate along $\langle 1\bar{2}10\rangle$ direction is usually higher than that along $\langle 10\bar{1}0\rangle$ directions, while both of them are higher than that along ⟨0001⟩ direction, therefore, the hexagonal plate-like particles with $(10\bar{1}0)$ and (0001) faces as well as small height-to-diameter ratio are usually formed [28]. After addtion of 1 wt.% Al, although the morphology of ZrB_2 has not changed too much and most of particles are still hexagonal plates, more particles with smaller size have been formed as shown in Figs. 7(b) and 8(b). The mean size of ZrB_2 in the Cu−1Al−3.15Zr−0.75B composite has decreased to about 1.57 μm, indicating that Al has a refinement effect on ZrB_2. The refinment effect of Al on ZrB_2 size is more significant when increasing Al addition amount. It

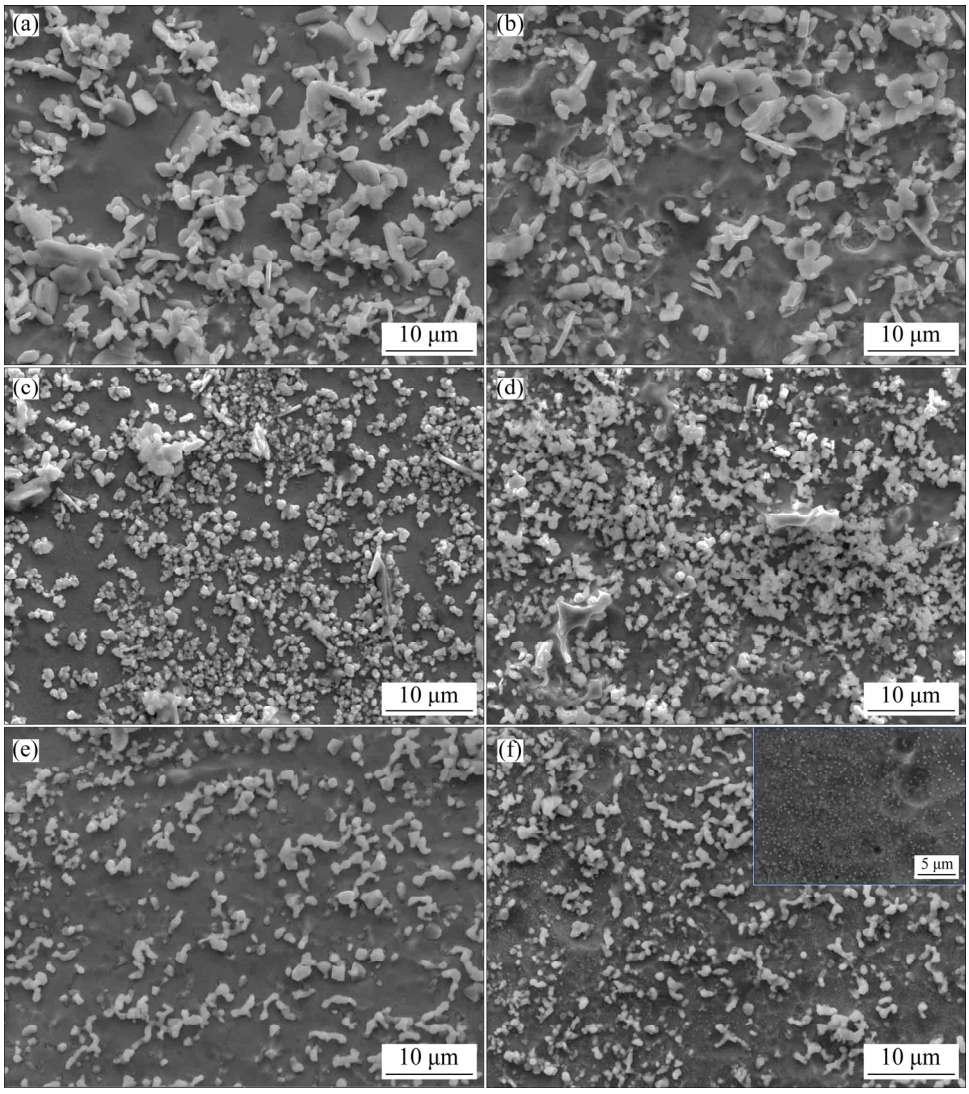

Fig. 7 Morphologies of in-situ synthesized ZrB_2 particles in different composites: (a) Cu−3.15Zr−0.75B; (b) Cu−1Al−3.15Zr−0.75B; (c) Cu−2Al−3.15Zr−0.75B; (d) Cu−3Al−3.15Zr−0.75B; (e) Cu−4Al−3.15Zr−0.75B; (f) Cu−6Al−3.15Zr−0.75B (Insert figure: synthesized small ZrB_2 particles)

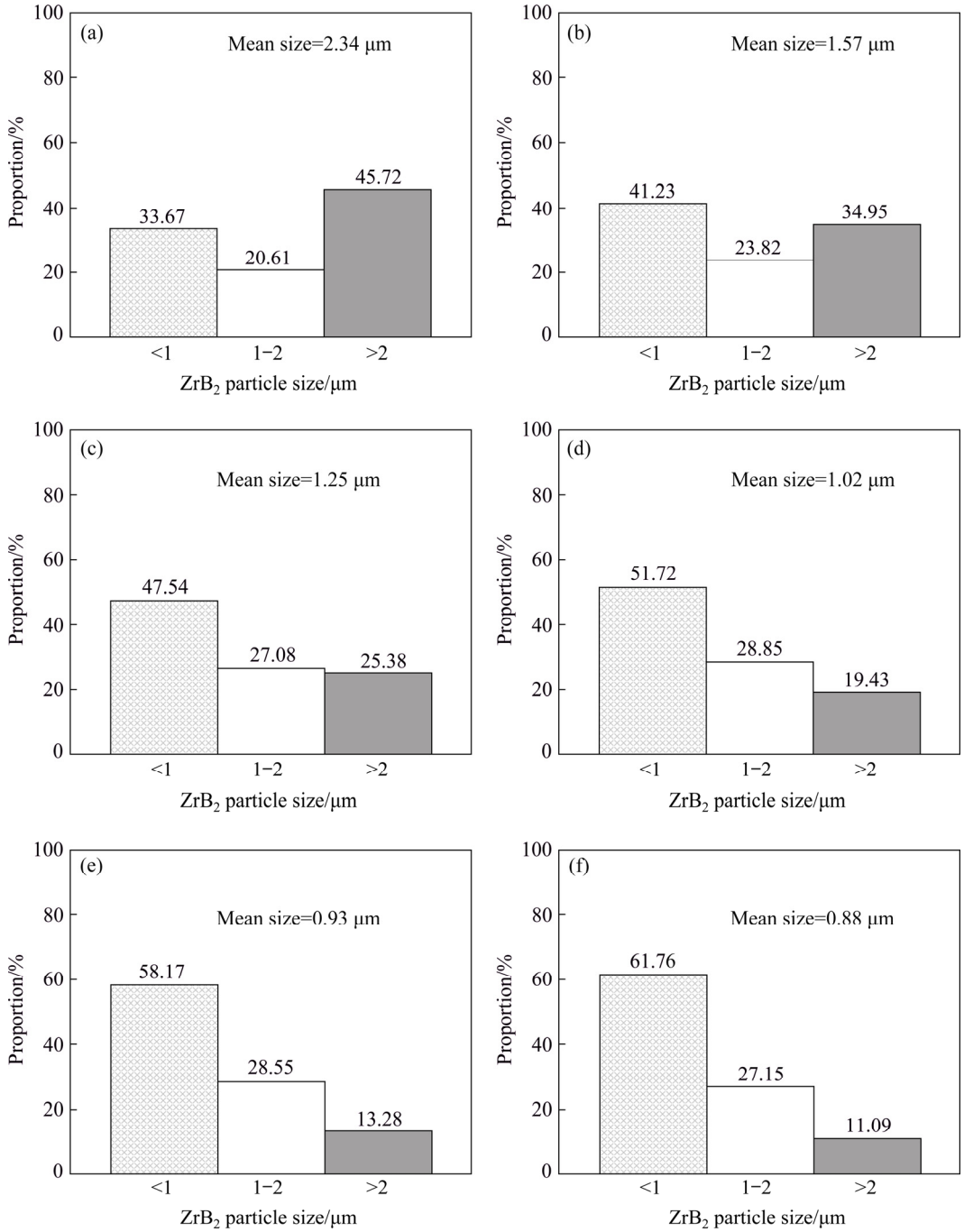

Fig. 8 Size and distribution of ZrB_2 particles in Cu−3.15Zr−0.75B (a), Cu−1Al−3.15Zr−0.75B (b), Cu−2Al−3.15Zr−0.75B (c), Cu−3Al−3.15Zr−0.75B (d), Cu−4Al−3.15Zr−0.75B (e) and Cu−6Al−3.15Zr−0.75B (f)

can be seen from Fig. 8 that the proportion of ZrB_2 particles larger than 2 μm decreases from about 45.72% to 11.09% with Al content increasing from 0 wt.% to 6 wt.%, while that of ZrB_2 particles less than 1μm increasing from about 33.67% to 61.76%. Some ZrB_2 particles with size smaller than 200 nm, even smaller than 100 nm have also be synthesized in Al-containing composities as shown in the insert of Fig. 7(f). As a result, the mean sizes of ZrB_2 decrease to about 1.25, 1.02, 0.93 and 0.88 μm in Cu−2Al−3.15Zr−0.75B, Cu−3Al−3.15Zr−0.75B, Cu−4Al−3.15Zr−0.75B and Cu−6Al−3.15Zr−0.75B compoistes, respectively. In addition, it is also found from Figs. 7(c−f) that the morphologies of ZrB_2 are also been modified. Many particles in Cu−*x*Al−3.15Zr−0.75B (*x*=2, 3, 4 or 6) are not plate-like but changed into polyhedron-like, even nearly sphere-like, as shown in Figs. 7(e, f).

Based on the above results, it can be sure that Al can significantly improve the distribution of in-situ synthesized ZrB_2 while refine the particle size and modify the morphlogy. The results given in Section 3.1 confim that there are no Al-containg particles which can act as nucleation sites for B phase in the Cu−2Al−0.75B melts. However, the modification effect of Al on ZrB_2 is already significant in Cu−2Al−3.15Zr−0.75B composites. Therefore, the modification effects of Al on ZrB_2 should mainly contribute to the restricted growth effect. It is deduced that, like the modification of Al on eutectic B, Al tends to adsorp on ZrB_2 surfaces which will retard the growth. The ZrB_2 morpologyies changed from hexagonal plate to polyhedron-like, even nearly sphere-like, indicating that the adsoption of Al should be selective, which means that the Al adsoption tendency on different ZrB_2 planes is varied.

In order to confirm the above deduction, the first-principles calculations based on the density-functional theory (DFT) used and the program package CASTEP were performed to examine the adsorption of Al on ZrB_2 (0001) basal plane, ZrB_2 $(10\bar{1}0)$ edge plane and ZrB_2 $(1\bar{2}10)$ plane. The generalized gradient approximation (GGA) of Perdew and Wang (PW91) was utilized for energy calculation. As mentioned above, ZrB_2 was an AlB_2-type crystal structure, which consisted of alternate stacking of a graphitelike boron layer and a close-packed metal layer [29]. Therefore, both the ZrB_2 (0001) and ZrB_2 $(10\bar{1}0)$ planes may be terminated by either the Zr layer or B layer, while ZrB_2 $(1\bar{2}10)$ planes contain both Zr and B atoms. However, it was confirmed by many works that ZrB_2 (0001) is usually terminated with the Zr layer [30,31]. Therefore, the Zr teminated ZrB_2 (0001) and ZrB_2 $(10\bar{1}0)$ planes along with ZrB_2 $(1\bar{2}10)$ plane which were all with a slab of 6-layers and 20 Å of vacuum region in the *z*-direction were used. The adsorption of Al on the most possible positions, including the top, bridge and the center sites of ZrB_2 (0001) and ZrB_2 $(10\bar{1}0)$ planes, and Zr as well as B top sites and the center site of ZrB_2 $(1\ \bar{2}\ 10)$, was calculated. The calculated Al adsorption sites were designated as Positions 1, 2 and 3, as shown in Fig. 9. During the structural optimization, atoms in the two bottom layers of each slab were kept fixed at their bulk-like positions, whereas atoms in other layers were fully relaxed and the plane-wave cut off energy of 380 eV was employed.

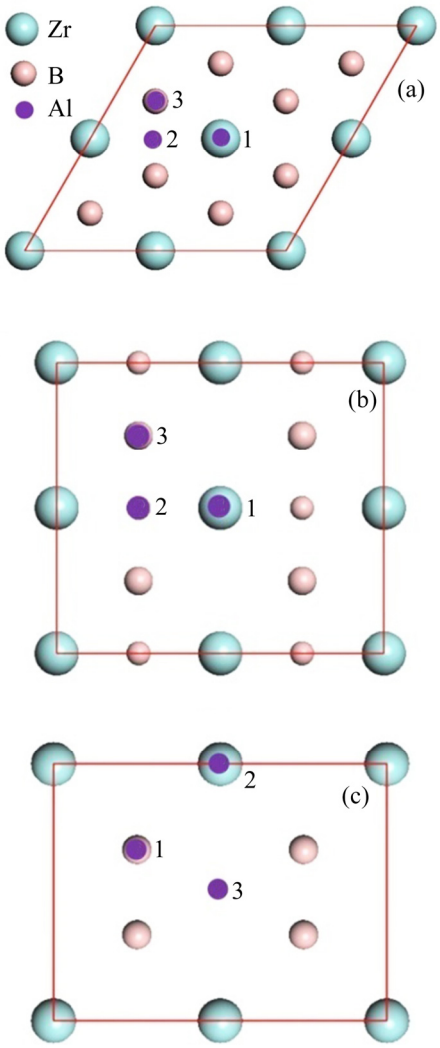

Fig. 9 Possible sites for Al adsorption on different ZrB_2 planes: (a) (0001); (b) $(10\bar{1}0)$; (c) $(1\bar{2}10)$ (The possible sites for Al adsorption are designated as Positions 1, 2 and 3)

The adsorption energies were then calculated by

$$E_{ads} = E_{Al+ZrB_2} - (E_{ZrB_2} + E_{Al}) \quad (1)$$

where E_{Al+ZrB_2} is the total energy of the ZrB_2 (0001), ZrB_2 $(10\bar{1}0)$ or ZrB_2 $(1\bar{2}10)$ plane with a Al atom, E_{ZrB_2} is the total energy of relaxed ZrB_2 (0001), ZrB_2 $(10\bar{1}0)$ or ZrB_2 $(1\bar{2}10)$ plane, E_{Al} is the energy of single Al atom calculated by placing it in a large enough box.

The calculated results are shown in Table 1. It can be seen that the adsorption energies of the Al atom on all the calcualted sites are negative,

indicating that it is theremally favorable for Al adsorption on ZrB_2 surfaces. It is found that Position 3 which has the largest adsorption energy is the most preferrd Al adsorption position in all the planes. In addition, the results also demonstrate that the adsoption of Al on ZrB_2 surfaces is selective. The Al atom is more preferentially adsobed on ZrB_2 $(1\bar{2}10)$ planes with the largest adsorption energy of −5.21 eV, then on the ZrB_2 $(10\bar{1}0)$ with the medium adsorption energy of −4.38 eV, and finally on the ZrB_2 (0001) planes with the smallest adsorption energy of −4.13 eV. The calculation results confirm the deduction that the modificaiton effects of Al on ZrB_2 mainly contribute to the restricted growth effect by Al selective adsorption on ZrB_2 surface. As mentioned above, before Al additon, the growth rate along ZrB_2 $\langle 1\bar{2}10\rangle$ direction is higher than that along $\langle 10\bar{1}0\rangle$ direction, while both of them are higher than that along ⟨0001⟩ direction. After Al addition, the growth rates along all the directions will be decreased due to the Al adsorption. Moreover, due to the selective adsorption, the growth rate decreases most along ZrB_2 $\langle 1\bar{2}10\rangle$ direction, while the least along ⟨0001⟩ direction. As a result, smaller sized ZrB_2 with polyhedron-like, even nearly sphere-like morphology, can be formed. Because the fast growth of ZrB_2 is also the main reasom for aggregation, the restricted growth effect of Al will also imporve the ZrB_2 distribution.

Table 1 Adsorption energies of Al on ZrB_2(0001), ZrB_2 $(10\bar{1}0)$ and ZrB_2 $(1\bar{2}10)$ (eV)

Adsorption site	ZrB_2(0001)	$ZrB_2$$(10\bar{1}0)$	$ZrB_2$$(1\bar{2}10)$
Position 1	−3.38	−2.90	−4.51
Position 2	−4.02	−3.20	−2.36
Position 3	−4.13	−4.38	−5.21

Due to the addition of Al and its improvement effects on the microstructures, the mechanical properties of Cu−ZrB_2 composites will be enhanced. However, because most of Al is dissovle in the Cu matrix, the electrical conductivity of the composites is inevitablely reduced. As shown in Fig. 10, the hardness of the composites has a great increase due to the addtion of Al, but the electrical conductivity of the Cu−3.15Zr−0.75 composites is decreased from 56.3% IACS to only 14.1% IACS with the addition of Al increasing from 0 wt.% to 6 wt.%. This is a problem for developing Cu matrix composites with both high strength and electrical conductivity and additional measures are needed to solve it in the furture.

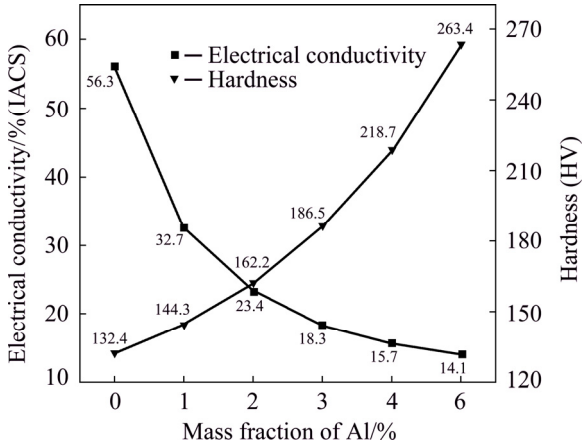

Fig. 10 Hardness and electrical conductivity of prepared Cu−*x*Al−3.15Zr−0.75B composites

4 Conclusions

(1) For Cu−B master alloys, Al has a significant modification effect on eutectic B and strong induction effect on the formation of primary B. With sufficient Al, the coarse needle-like eutectic B will be changed into fine fibrous structure, and primary B will be formed in hypoeutectic Cu−B alloys. It is considered that Al adsorption on the growth surface of the eutectic B and the formation of Al-containing particles which can be nucleation sites for the primary B are the reasons for the modification.

(2) When preparing Cu−ZrB_2 compsites by in-situ synthesizing ZrB_2 in the melts, the additon of Al into Cu−B melts can significantly improve the distribution of ZrB_2 and refine them as well as modify the morphlogy. The effect is more significant with increase of Al content.

(3) The effect of Al on ZrB_2 is due to its selective adsorption on ZrB_2 surfaces. It is calculted that it is thermally favorable for Al adsorption on ZrB_2 surface. Morover, Al is preferentially adsobed on the ZrB_2 $(1\bar{2}10)$ plane, then on the ZrB_2 $(10\bar{1}0)$, and finally on the ZrB_2 (0001) plane. As a result, smaller sized ZrB_2 with a polyhedron-like, even nearly sphere-like morphology, can be formed.

(4) Due to Al addition and its modificaton effects, the hardness of Cu−ZrB_2 composites is greatly enhanced, but the electrical conductivity of the composites is seriously reduced.

References

[1] CHEN Xiao-hong, ZHOU Hong-lei, ZHANG Tao, BI Li-ming, TIAN Wei, FU Shao-li, LI Wei, LIU Xin-kuan, MA Feng-cang, ZHANG Ke, SUN Hao, LIU Ping. Mechanism of interaction between the Cu/Cr interface and its chemical mixing on tensile strength and electrical conductivity of a Cu−Cr−Zr alloy [J]. Materials & Design, 2019, 180: 107976.

[2] WANG Lin, DU Qing-lin, LI Chang, CUI Xiao-hui, ZHAO Xing, YU Hai-liang. Enhanced mechanical properties of lamellar Cu/Al composites processed via high-temperature accumulative roll bonding [J]. Transactions of Nonferrous Metals Society of China, 2019, 29:1621−1630.

[3] UCHIDA S, KIMURA T, NAKAMOTO T, OZAKI T, MIKI T, TAKEMURA M, OKA Y, TSUBOTA R. Microstructures and electrical and mechanical properties of Cu−Cr alloys fabricated by selective laser melting [J]. Materials & Design 2019, 175: 107815.

[4] TORABI H, ARGHAVANIAN R. Investigations on the corrosion resistance and microhardness of Cu−10Sn/SiC composite manufactured by powder metallurgy process [J]. Journal of Alloys and Compounds, 2019, 806: 99−105.

[5] ZHANG Yin-yin, CHOUDHURI D, SCHARF T W, DESCARTES S, CHROMIK R R. Tribologically induced nanolaminate in a cold-sprayed WC-reinforced Cu matrix composite: A key to high wear resistance [J]. Materials & Design, 2019, 182: 108009.

[6] NALEPKA K, SZTWIERTNIA K, NALEPK P. Preferred orientation relationships at the Cu/α−Al_2O_3 interface: Identification and theoretical explanation [J]. Acta Materialia, 2016, 104: 156−165.

[7] YU Hao-yang, FANG Wei, CHANG Ruo-bin, JI Pu-guang, WANG Qing-zhou. Modifying element diffusion pathway by transition layer structure in high-entropy alloy particle reinforced Cu matrix composites [J]. Transactions of Nonferrous Metals Society of China, 2019, 29: 2331−2339.

[8] LEE D W, HA G H, KIM B K. Synthesis of Cu−Al_2O_3 nano composite powder [J]. Scripta Materialia, 2001, 44: 2137−2140.

[9] CABEZAS-VILLA J L, OLMOS L, VERGARA-HERNÁNDEZ H J, JIMÉNEZ O, GARNICA P, BOUVARD D, FLORES M. Constrained sintering and wear properties of Cu−WC composite coatings [J]. Transactions of Nonferrous Metals Society of China, 2017, 27: 2214−2224.

[10] JAVADHESARI S M, ALIPOUR S, AKBARPOUR M R. Microstructural characterization and enhanced hardness, wear and antibacterial properties of a powder metallurgy SiC/Ti−Cu nanocomposite as a potential material for biomedical applications [J]. Ceramics International, 2019, 45: 10603−10611.

[11] MANSOURZADEH S, HOSSEINI M, SALAHINEJAD E, YAGHTIN A H. Cu−$(B_4C)_p$ metal matrix composites processed by accumulative roll-bonding [J]. Progress in Natural Science-Materials International, 2016, 26: 613−620.

[12] MONTEVERDE F, BELLOSI A, GUICCIARDI S. Processing and properties of zirconium diboride-based composites [J]. Journal of the European Ceramic Society, 2002, 22: 279−288.

[13] YU Zhu-li, ZHU He-guo, HUANG Jie-wei, LI Jian-liang, XIE Zong-han. Processing and characterization of in-situ ultrafine TiB_2−Cu composites from Ti−B−Cu system [J]. Powder Technology, 2017, 320: 66−72.

[14] LEE J S, KIM N J, JUNG J Y, LEE E S, AHN S. The influence of reinforced particle fracture on strengthening of spray formed Cu−TiB_2 composite [J]. Scripta Materialia, 1998, 39: 1063−1069.

[15] YE You-xiong, YANG Xu-yue, WANG Jun, ZHANG Xiang-kai, ZHANG Zhi-ling, SAKAI T K. Enhanced strength and electrical conductivity of Cu−Zr−B alloy by double deformation-aging process [J]. Journal of Alloys and Compounds, 2014, 615: 249−254.

[16] RUZIC J, STASIC J, RAJKOVIC V, BOZIC D. Synthesis, microstructure and mechanical properties of ZrB_2 nano and micro particle reinforced copper matrix composite by in situ processings [J]. Materials & Design, 2014, 62: 409−415.

[17] PASSERONE A, MUOLO M L, NOVAKOVIC R, PASSERONE D. Liquid metal/ceramic interactions in the (Cu,Ag,Au)/ZrB_2 systems [J]. Journal of the European Ceramic Society, 2007, 27: 3277−3285.

[18] MISHRA S K, DAS S K, SHERBACOV V. Fabrication of Al_2O_3−ZrB_2 in situ composite by SHS dynamic compaction: A novel approach [J]. Composites Science Technology, 2007, 67: 2447−2453.

[19] ZHANG Zhi-guo, SHENG Yin-ying, XU Xi-wei, LI Wei. Microstructural features and mechanical properties of in situ formed ZrB_2/Cu composites [J]. Advanced Engineering Materials, 2015, 17: 1338−1343.

[20] WANG Chen-chen, LIN Huai-jun, ZHANG Zhiguo, LI Wei. Fabrication, interfacial characteristics and strengthening mechanisms of ZrB_2 microparticles reinforced Cu composites prepared by hot-pressed sintering [J]. Journal of Alloys and Compounds, 2018, 748: 546−522.

[21] STASIC J, RAJKOVIC V, RUZIC J, BOZIC D. An investigation on synthesis development of high hardened, high conductivity Cu−Zr and Cu−Zr−ZrB_2 alloys through green compact laser sintering [J]. International Journal of Advanced Manufacturing Technology, 2015, 80: 1049−1057.

[22] FAN Xiao-liang, HUANG Xiao-wei, LIU Qing, DING Hai-min, WANG Hui-qiang, HAO Ce. The microstructures and properties of in-situ ZrB_2 reinforced Cu matrix composites [J]. Results in Physics, 2019, 14: 102494.

[23] WU Yu-ying, LI Chong, LIU Xiang-fa, LU Kai. In situ formation of super hard C-B based composite by reducing reaction [J]. Journal of Alloys and Compounds, 2012, 527: 184−187.

[24] LIU Xiao-rui, ZHANG Yu-dong, BEAUSIR B, LIU Fang, ESLING C, YU Fu-xiao, ZHAO Xiang, ZUO Liang. Twin-controlled growth of eutectic Si in unmodified and Sr-modified Al−12.7%Si alloys investigated by SEM/EBSD [J]. Acta Materialia, 2015, 97: 338−347.

[25] TIMPEL M, WANDERKA N, SCHLESIGER R, YAMAMOTO T, LAZAREV N, ISHEIM D, SCHMITZ G, MATSUMURA S, BANHART J. The role of strontium in modifying aluminium−silicon alloys [J]. Acta Materialia, 2012, 60: 3920−3928.

[26] LIU Xiang-fa, WU Yu-ying, BIAN Xiu-fang. The nucleation

sites of primary Si in Al−Si alloys after addition of boron and phosphorus [J]. Journal of Alloys and Compounds, 2005, 391: 90−94.

[27] LIANG Song-mao, SCHMID-FETZER R. Phosphorus in Al−Si cast alloys: Thermodynamic prediction of the AlP and eutectic (Si) solidification sequence validated by microstructure and nucleation undercooling data [J]. Acta Materialia, 2014, 72: 41−56.

[28] VALLAURI D, ATIAS ADRIAN IC, CHRYSANTHOU A. TiC−TiB_2 composites: A review of phase relationships, processing and properties [J]. Journal of the European Ceramic Society, 2008, 28: 1697−1713.

[29] MAGNUSON M, TENGDELIUS L, GRECZYNSKI G, HULTMAN L, HOGBERG H. Chemical bonding in epitaxial ZrB_2 studied by X-ray spectroscopy [J]. Thin Solid Films C, 2018, 649: 89−96.

[30] AIZAWA T, SUEHARA S, HISHITA S, OTANI S. Surface core-level shift and electronic structure on transition-metal diboride (0001) surfaces [J]. Physical Review B, 2005, 71: 165405.

[31] AIZAWA T, HAYAMI W, OTANI S. Surface phonon dispersion of ZrB_2 (0001) and NbB_2 (0001) [J]. Physical Review B, 2002, 65: 024303.

Al 的添加对 Cu−B 合金及 Cu−ZrB_2 复合材料显微组织的影响

丁海民[1]，苗文智[1]，黄小伟[1]，柳 青[1]，范孝良[1]，王会强[2]，储开宇[1]，李春燕[1]

1. 华北电力大学 能源动力与机械工程学院，保定 071003；
2. 河北农业大学 机电工程学院，保定 071001

摘 要：采用扫描电子显微镜、X 射线衍射以及第一性原理计算方法研究 Al 的添加对 Cu−B 合金及 Cu−ZrB_2 复合材料显微组织的影响。结果表明，在 Al 的变质作用下，Cu−B 合金中的共晶 B 相由粗大针状转变为细小纤维状，同时可以在亚共晶 Cu−B 合金中析出初生 B 相。对于 Cu−ZrB_2 复合材料，Al 能够细化合成的 ZrB_2 颗粒，改变其形貌，同时改善其分布，这归因于 Al 在 ZrB_2 晶面上的选择性吸附。第一性原理计算表明，Al 会优先吸附在 $ZrB_2(1\bar{2}10)$面上，其次是 $ZrB_2(10\bar{1}0)$面，最后是 ZrB_2 (0001)面，进而使复合材料中形成多面体状、乃至近球状细小 ZrB_2 颗粒。Al 的加入使 Cu−ZrB_2 复合材料硬度显著提高，但其电导率严重降低。

关键词：Cu−B 合金；铜基复合材料；变质作用；显微组织

(Edited by Xiang-qun LI)